

Analysis of the anomalous doppler effect from quantum theory to classical dynamics simulations

Xinhang Xu(徐新航)¹, Jinlin Xie(谢锦林)^{1,†}, Jian Liu(刘健)², and Wandong Liu(刘万东)¹

¹Department of Plasma Physics and Fusion Engineering, University of Science and Technology of China, Hefei 230026, China

²Weihai Institute for Interdisciplinary Research, Shandong University, Weihai 264209, China

(Received 12 May 2025; revised manuscript received 13 June 2025; accepted manuscript online 27 June 2025)

The fundamental physics of anomalous and normal Doppler resonances between electrons and electromagnetic waves is analyzed using a quantum model that incorporates angular-momentum conservation. This work extends prior theory by explicitly linking the resonant integer m to the EM wave's angular-momentum quantum number, as shown in 2. Numerical simulations based on the volume-preserving algorithm (VPA) further confirm this correspondence. Moreover, a direct comparison of the energy-transfer ratio from translational energy to gyrokinetic energy during resonance, between classical dynamics and quantum predictions, is presented and verified numerically.

Keywords: anomalous doppler effect, resonant condition, angular momentum conservation

PACS: 03.65.-w, 33.35.+r, 02.60.Cb, 12.20.-m

DOI: [10.1088/1674-1056/ade8e4](https://doi.org/10.1088/1674-1056/ade8e4)

CSTR: [32038.14.CPB.ade8e4](https://cstr.iopscience.iop.org/32038.14.CPB.ade8e4)

1. Introduction

The anomalous Doppler effect (ADE),^[1,2,4,5] in which the observed frequency shift behaves contrary to the conventional Doppler effect under specific conditions, was first theoretically predicted by Soviet physicist Ginzburg.^[4] This phenomenon arises when a system moves with a velocity exceeding the phase velocity of light in the medium, transferring its translational kinetic energy into internal energy while emitting radiation. A notable example, discussed by Frank in his 1958 Nobel lecture,^[2] shows that radiation emission does not occur through the typical transition from an excited state to a lower energy level. Instead, it proceeds from a lower to a higher energy level, powered by the system's translational kinetic energy. This counterintuitive prediction has attracted considerable attention and has inspired extensive research.^[6–8,10–14]

In 1967, Artsimovich^[15] reported discrepancies in tokamak experiments: the electron temperature estimated from diamagnetic signals was significantly higher than that derived from electrical-conductivity measurements. Although unrecognized at the time, this anomaly may represent the first experimental observation of ADE. In 1968, Kadomtsev^[16] identified ADE as the underlying mechanism, in which electrons undergo velocity scattering from the longitudinal to the transverse direction under resonant conditions. This process enhances the diamagnetic effect beyond what would be expected from thermal motion alone. Subsequently, a range of ADE-related phenomena have been observed, including electron-beam scattering in magnetic-field vacuum tubes,^[2] wave radiation,^[17–19] and runaway-electron instabilities in tokamaks.^[20,21] The ADE has also given rise to practical ap-

plications, notably in high-power microwave generation and in mitigating runaway electrons in tokamak fusion reactors.^[11,22]

The physics of the ADE was first elucidated through quantum analysis by Frank and Ginzburg.^[2,23] In this work, we extend Ginzburg's quantum framework by incorporating the conservation of angular momentum to provide a more rigorous analysis of ADE. This approach yields new insights into the relationship between wave angular momentum and ADE under resonant conditions, which is referred to as anomalous Doppler resonance (ADR). For an electron moving in a magnetic field and interacting with an external electromagnetic (EM) wave, the general resonance condition is given by

$$\omega = m\omega_{ce} + \mathbf{k} \cdot \mathbf{v},$$

where \mathbf{k} is the wave vector, ω_{ce} is the electron cyclotron frequency (here $\omega_{ce} > 0$), \mathbf{v} is the electron velocity, and ω is the wave angular frequency, while $m = 0, \pm 1, \pm 2, \pm 3, \dots$ represents the Landau level.^[26] Specifically, for plane EM waves, we find that resonance is restricted to the fundamental harmonics ($m = \pm 1$) due to spin angular-momentum conservation, reducing the condition to

$$\omega = \pm \omega_{ce} + \mathbf{k} \cdot \mathbf{v},$$

where the negative sign refers to the ADR condition, while the positive sign refers to the normal Doppler resonance (NDR) condition. This represents a significant constraint compared to previous theoretical treatments^[41] which suggested possible resonance at all harmonic orders ($m = \pm 1, \pm 2, \dots$). Despite the simplicity of the model, our analysis demonstrates that angular-momentum conservation plays a crucial role in

[†]Corresponding author. E-mail: jlxie@ustc.edu.cn

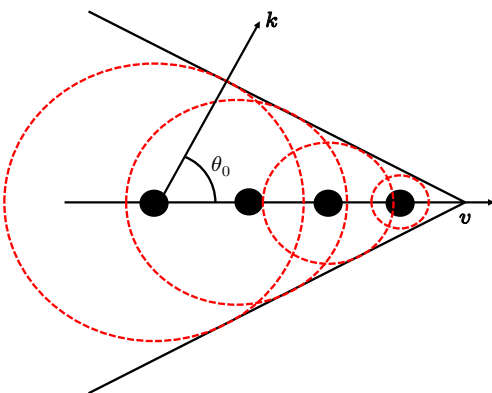
67 EM wave-electron resonance — an aspect that, to the best of
 68 our knowledge, has not been previously addressed in the liter-
 69 ature.

70 Furthermore, we perform numerical simulations of a sin-
 71 gle electron interacting resonantly with an EM wave in the
 72 presence of uniform static electric and magnetic fields, us-
 73 ing classical equations of motion. These simulations eluci-
 74 date the relationship between wave angular momentum and the
 75 resonance mechanism. Additionally, we compute the energy-
 76 transfer ratio from the electron's translational kinetic energy to
 77 its gyrokinetic energy during resonance, and the results show
 78 strong agreement with predictions from quantum theory.

79 The remainder of this paper is organized as follows. Sec-
 80 tion 2 develops the quantum theoretical framework incorpo-
 81 rating angular-momentum conservation. Section 3 presents
 82 our numerical approach, detailing the simulation setup, ana-
 83 lyzing the time evolution of electron velocity and kinetic en-
 84 ergy, investigating the resonant conditions with wave angular
 85 momentum, and examining the energy-transfer ratio and po-
 86 larization characteristics. Section 4 provides a comprehensive
 87 discussion of the key findings and their physical implications.
 88 Finally, Section 5 summarizes the principal conclusions and
 89 outlines potential directions for future research.

90 2. Quantum analysis of ADE

91 When a charged particle moves through a medium at a
 92 speed greater than the phase velocity of light in that medium,
 93 it induces polarization in the surrounding molecules. As these
 94 molecules return to their equilibrium state, they emit elec-
 95 tromagnetic radiation. The constructive interference of these
 96 emissions produces the characteristic Cherenkov radiation,
 97 forming a cone-shaped wavefront, as shown in Fig. 1. The di-
 98 rection of Cherenkov radiation is constrained to the Cherenkov
 99 radiation angle $\theta_0 = \arccos\left(\frac{c'}{v}\right)$, where c' is the speed of light
 100 in the medium and v is the velocity of the charged particle.



101 **Fig. 1.** Schematic diagram of Cherenkov radiation. The black points in-
 102 dicate snapshots of the electron at different times, the red dashed circle
 103 represents the current radiation surface from the previous electron.

104 However, when the electron is replaced by a system pos-
 105 sessing internal energy — such as an oscillator or a cyclotron

105 electron in a magnetic field — the direction of the emitted pho-
 106 ton is no longer determined by the interference of secondary
 107 waves and can instead occur in any direction. Considering a
 108 scenario in which the system emits a photon with angular fre-
 109 quency ω and wavevector k , the emission process must satisfy
 110 both energy and momentum conservation:

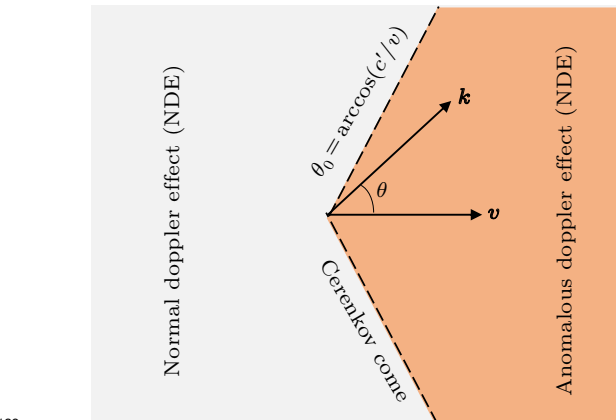
$$111 \quad T_1 + U_1 = \hbar\omega + T_2 + U_2, \quad (1a)$$

$$112 \quad p_1 = p_2 + \hbar k. \quad (1b)$$

113 Here, T and U represent the kinetic energy and internal
 114 energy of the system, while the subscripts 1 and 2 refer to the
 115 states before and after emitting a photon. p denotes the mo-
 116 mentum of the system, and \hbar represents the reduced Planck
 117 constant. Assuming that the photon's energy is far less than
 118 the initial kinetic energy T_1 , the loss of kinetic energy after
 119 photon emission can be written as $\Delta T_{12} = T_1 - T_2 = \Delta p \cdot v$,
 120 where v is the velocity of the system before emission and
 121 $\Delta p = p_1 - p_2 = \hbar k$. Thus, the change in internal energy be-
 122 comes

$$123 \quad \Delta U_{21} = \Delta T_{12} - \hbar\omega = \hbar k \cdot v - \hbar\omega = \hbar\omega \left(\frac{v \cos \theta}{c'} - 1 \right). \quad (2)$$

124 Here, $\omega/k = c'$, and $\Delta U_{21} = U_2 - U_1$. When the system's ve-
 125 locity exceeds the speed of light in the medium ($v > c'$), the
 126 sign of ΔU_{21} allows the radiation to be categorized into three
 127 distinct regions, as illustrated in Fig. 2.



128 **Fig. 2.** Regions of the ADE and the NDE .

129 (i) For $\theta > \theta_0 = \arccos(c'/v)$, $\Delta U_{21} < 0$. The system
 130 produces photons by consuming both its internal and kinetic
 131 energy; this region corresponds to the normal Doppler effect
 132 (NDE).

133 (ii) For $\theta = \theta_0$, $\Delta U_{21} = 0$, and the loss of kinetic energy
 134 by the system is completely converted into photon energy; this
 135 line corresponds to the Cherenkov Effect.

136 (iii) For $\theta < \theta_0$, $\Delta U_{21} > 0$. This region is referred to as
 137 the ADE, where the system gains internal energy after emit-
 138 ting photons. This means that the loss of kinetic energy is
 139 converted into both photon energy and internal energy.

In previous work, the change in internal energy was given as $\Delta U = m\hbar\omega_{ce}$, where $m = 0, \pm 1, \pm 2, \pm 3, \dots$ represents the Landau level, as reported by Ginzburg,^[25] Coppi,^[26] Frolov,^[27] Frank,^[2] Tamm^[1] and Nezlin.^[6] The above discussion revisits the foundational work of Ginzburg.^[25] In the present paper, it is further demonstrated that m actually corresponds to the quantum number associated with the angular momentum of the emitted photon.

Let us consider the process in which an electron cyclotron system under a uniform magnetic field emits a photon along the z axis, as shown in Fig. 3. The moving electron has velocity v_z along the background magnetic field and cyclotron velocity v_{\perp} . The kinetic energy along z is $T = \gamma m_e c^2 - m_e c^2$, where γ denotes the Lorentz factor. The internal energy is expressed as $U = \frac{1}{2} \gamma m_e v_{\perp}^2$.

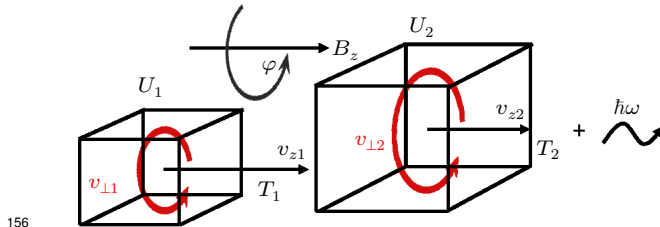


Fig. 3. Schematic diagram of the electron cyclotron system before and after photon emission. Here, $U_2 > U_1$ and $T_2 < T_1$.

Assume the angular momentum of the system before and after emitting a photon is L_1 and L_2 , respectively. The angular momentum of the photon is $m\hbar$. According to angular-momentum conservation, we have

$$L_1 = L_2 + m\hbar. \quad (3)$$

Since the magnetic field is aligned along the z direction, the angular momentum of the electron along z is represented as L_z . According to quantum theory, the electron wave in a static magnetic field can be expressed as

$$\Psi = \Psi_0 e^{\frac{i}{\hbar} (\mathbf{p} - e\mathbf{A}) \cdot \mathbf{s}}, \quad (4)$$

where Ψ_0 is the normalization coefficient, \mathbf{A} is the vector potential, and \mathbf{s} is the position. For a gyrating electron in a magnetic field, $\mathbf{s} = r\phi \mathbf{e}_\phi$, where r is the cyclotron radius and ϕ is the cyclotron angle.

The z -component of the orbital angular momentum operator can be expressed in spherical coordinates as

$$\hat{L}_z = -i\hbar \frac{\partial}{\partial \phi}. \quad (5)$$

Combining Eq. (4) with Eq. (5), we have

$$-i\hbar \frac{\partial}{\partial \phi} \Psi = (p_\phi - eA_\phi) r \Psi. \quad (6)$$

As a result, the eigenvalue of L_z can be expressed as

$$L_z = (p_\phi - eA_\phi)r. \quad (7)$$

With $p_\phi = \gamma m_e v_{\perp}$, $A_\phi = \frac{rB_0}{2}$, and $r = \frac{\gamma m_0 v_{\perp}}{B_0 e}$, Eq. (7) can be rewritten as

$$L_z = \frac{1}{2} \cdot \frac{\gamma m_0 v_{\perp}^2}{\omega_{ce}} = \frac{U}{\omega_{ce}}, \quad (8)$$

where $\omega_{ce} = \frac{eB}{m_0 \gamma} = \frac{\omega_0}{\gamma}$ and $U = \frac{1}{2} \gamma m_0 v_{\perp}^2$. Here, m_0 is the electron rest mass, γ is the Lorentz factor, and ω_0 is the electron cyclotron frequency in the rest frame (here we choose $\omega_0 > 0$). The conservation of angular momentum in the z -direction is expressed as

$$L_{z2} + m\hbar = L_{z1}. \quad (187)$$

The variation in the angular momentum of the electron along the z -axis is given by

$$\Delta L_{21} = L_{z2} - L_{z1} = \frac{U_2 - U_1}{\omega_{ce}} = -m\hbar. \quad (9)$$

Here, m is the quantum number of the photon's angular momentum in the z -direction. The internal-energy change is given by $\Delta U_{21} = U_2 - U_1$. With Eq. (9), it can be rewritten as

$$\Delta U_{21} = -m\hbar\omega_{ce}. \quad (10)$$

According to Eqs. (2) and (10), the change in electron energy can be written as

$$\hbar\mathbf{k} \cdot \mathbf{v} = \hbar\omega - m\hbar\omega_{ce}. \quad (11)$$

This result is consistent with previous findings.^[1,2,6,24,26,27] Here, $\hbar\mathbf{k} \cdot \mathbf{v}$ represents the loss of kinetic energy ΔT_{12} , $\hbar\omega$ represents the photon energy, and $-m\hbar\omega_{ce}$ represents the change in electron gyrokinetic energy ΔU_{21} . The ratio between the internal-energy change ΔU_{21} and the kinetic-energy change ΔT_{21} is

$$\frac{\Delta U_{21}}{\Delta T_{21}} = \frac{m\hbar\omega_{ce}}{\hbar\mathbf{k} \cdot \mathbf{v}}. \quad (12)$$

This result is a critical criterion for comparison with the classical dynamic simulation in Section 2. It is also derived from classical theory in the Appendix. After simplifying Eq. (11), we finally obtain the classical wave-particle resonance condition

$$\omega = k_z v_z + m\omega_{ce}. \quad (13)$$

The variable m represents the quantum number associated with the angular momentum of the photon. Since a photon possesses both orbital angular momentum ($l\hbar$, where $l = 0, \pm 1, \pm 2, \pm 3, \dots$) and intrinsic spin angular momentum ($s\hbar$, where $s = \pm 1$),^[28] the total angular momentum can be expressed as $m\hbar = l\hbar + s\hbar$.

217 For photons carrying only spin angular momentum, two
 218 distinct quantum states are possible, characterized by the spin
 219 quantum number m :

220 (i) For $m = +1$ ($\Delta U_{21} < 0$), the cyclotron electron loses
 221 internal energy upon photon emission. The emitted photon ex-
 222 hibits right-hand circular polarization. This process is known
 223 as the NDE.

224 (ii) For $m = -1$ ($\Delta U_{21} > 0$), the cyclotron electron gains
 225 internal energy through photon emission. The emitted pho-
 226 ton exhibits left-hand circular polarization (the difference be-
 227 tween our definition of circular polarization and the standard
 228 definition^[3] stems from our choice of $\omega_0 > 0$. Here, $m > 0$
 229 corresponds to the same rotational sense as the electron's natu-
 230 ral right-hand gyration, yielding right-hand polarization when
 231 $\mathbf{k} \parallel \mathbf{B}_0$). This process corresponds to the ADE.

232 The above discussion describes spontaneous emission
 233 phenomena of ADE and NDE without external-field interven-
 234 tion. In our simulation model, we introduce an external plane
 235 EM wave that serves as a resonant field interacting with elec-
 236 trons. This plane EM wave acts as an inducing field, enabling
 237 a gyro-electron to undergo stimulated absorption or emission
 238 processes. From a quantum perspective, the plane EM wave
 239 can be regarded as an ocean of photons that carry only spin
 240 angular momentum. Consequently, the same resonance condi-
 241 tions as those derived from quantum field theory are recovered:

242 (i) Right-hand circularly polarized waves correspond to
 243 $m = +1$ states,^[39] resonating only when $\omega = \omega_{ce} + \mathbf{k} \cdot \mathbf{v}$ (NDE
 244 condition).

245 (ii) Left-hand circularly polarized waves correspond to
 246 $m = -1$ states, resonating only when $\omega = -\omega_{ce} + \mathbf{k} \cdot \mathbf{v}$ (ADE
 247 condition).

248 This exact correspondence between our classical simula-
 249 tion framework and quantum field-theoretic predictions vali-
 250 dates our modeling approach while providing physical insight
 251 into the angular-momentum selection rules governing these
 252 resonant interactions.

253 Although nonlinear analyses of electron interactions with
 254 electromagnetic waves have been extensively studied,^[29–37]
 255 the specific role of static electric fields in these interactions
 256 has received comparatively less attention. In our approach,
 257 the uniform electric field serves a crucial function by system-
 258 atically scanning the electron velocity, thereby enabling inves-
 259 tigation across the full spectrum of resonance conditions. The
 260 inherent complexity of these nonlinear processes precludes an-
 261 alytical solutions, necessitating the use of numerical simula-
 262 tion methods to obtain meaningful physical insights.

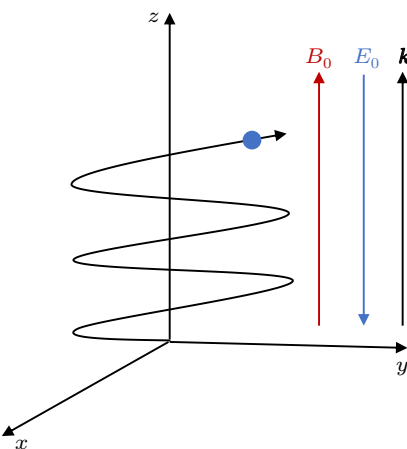
263 3. Classical dynamic simulation of ADR

264 The ADE process has been theoretically analyzed in the
 265 quantum framework, where the angular momentum carried by
 266 the emitted photon determines the resonance condition. To

267 validate these characteristics in a classical picture, we investi-
 268 gate the interaction between an electromagnetic wave and an
 269 electron during ADR and NDR. The corresponding energy-
 270 transfer ratio can also be examined through numerical simula-
 271 tions.

272 3.1. Numerical simulation setup

273 To analyze the resonant process from the perspective of
 274 classical dynamics and to facilitate a direct comparison with
 275 the quantum results, we consider the following configuration.
 276 A uniform magnetic field \mathbf{B}_0 is applied along the z -direction.
 277 An electrostatic field \mathbf{E}_0 , oriented opposite to \mathbf{B}_0 (as illus-
 278 trated in Fig. 4), is introduced to accelerate the electron.



279 **Fig. 4.** Schematic of the setup: a uniform static magnetic field B_0 along
 280 the z -axis, an electrostatic field E_0 oriented opposite to B_0 , and a wavevector k aligned parallel to B_0 .

281 We consider the interaction between an electron enter-
 282 ing the system with velocity v_z , parallel to the magnetic field
 283 $B_0 = B_z$, and a linearly or circularly polarized transverse elec-
 284 tromagnetic (TEM) wave propagating in a homogeneous di-
 285 electric medium with a refractive index $n > 1$.

286 The induced linearly polarized wave along B_0 can be de-
 287 composed into a combination of a right-hand circularly polar-
 288 ized wave ($m = 1$) and a left-hand circularly polarized wave
 289 ($m = -1$), such that $\mathbf{E}_w = \mathbf{E}_R + \mathbf{E}_L$, where $\mathbf{E}_R = \frac{1}{2}\mathbf{E}_0(e_x +$
 290 $i e_y) \exp[i(\mathbf{k} \cdot \mathbf{r} - \omega t)]$, $\mathbf{E}_L = \frac{1}{2}\mathbf{E}_0(e_x - i e_y) \exp[i(\mathbf{k} \cdot \mathbf{r} - \omega t)]$.
 291 The magnetic field of the EM wave is

$$292 \quad \mathbf{B}_w = \frac{\mathbf{k} \times \mathbf{E}_w}{\omega}. \quad (14)$$

293 The six-dimensional phase space of an electron, de-
 294 scribed by its position \mathbf{r} and momentum \mathbf{p} , is governed by
 295 the equations below. The vectors \mathbf{E} and \mathbf{B} represent the total
 296 field, including both static and electromagnetic components.
 297 Here, c denotes the speed of light in vacuum, e represents the
 298 electron's charge, and m_0 is the electron's rest mass

$$299 \quad \frac{d\mathbf{r}}{dt} = \frac{\mathbf{p}}{\sqrt{m_0^2 + \frac{\mathbf{p}^2}{c^2}}},$$

$$300 \quad \frac{dp}{dt} = -e \left(\mathbf{E}(\mathbf{r}, t) + \frac{\mathbf{p}}{\sqrt{m_0^2 + \frac{\mathbf{p}^2}{c^2}}} \times \mathbf{B}(\mathbf{r}, t) \right). \quad (15)$$

301 To simulate the evolution of \mathbf{r} and \mathbf{p} , the above system is
 302 discretized using the Volume-Preserving Algorithm.^[9,38] Let
 303 j denote the iteration step and $\text{Cay}(\mathbf{A})$ represent the Cayley
 304 transform of matrix \mathbf{A}

$$305 \quad \left\{ \begin{array}{l} \mathbf{r}_{j+\frac{1}{2}}^* = \mathbf{r}_j^* + \frac{\Delta t^*}{2\gamma_j} \mathbf{p}_j^*, \\ \mathbf{p}^{*-} = \mathbf{p}_j^* + \frac{\Delta t^*}{2} \mathbf{E}_{j+\frac{1}{2}}^*, \\ \mathbf{p}^{*+} = \text{Cay} \left(\frac{\Delta t^* \hat{\mathbf{B}}^*}{2\gamma_j} \right) \mathbf{p}^{*-}, \\ \mathbf{p}_{j+1}^* = \mathbf{p}^{*+} + \frac{\Delta t^*}{2} \mathbf{E}_{j+\frac{1}{2}}^*, \\ \mathbf{r}_{j+1}^* = \mathbf{r}_{j+\frac{1}{2}}^* + \frac{\Delta t^*}{2\gamma_{j+1}} \mathbf{p}_{j+1}^*. \end{array} \right. \quad (16)$$

306 The dimensionless parameters are momentum $p^* = p/(m_0 c)$,
 307 magnetic field $B^* = B/(e\tau_{ce} m_0)$, total electric field $E^* =$
 308 $E/[m_0 c/(\tau_{ce} e)]$, time step $\Delta t^* = \Delta t/\tau_{ce}$, and position $r^* =$
 309 $r/(\tau_{ce} c)$, where τ_{ce} is the electron cyclotron period ($\tau_{ce} =$
 310 $2\pi/\omega_{ce}$) and $\gamma^* = \sqrt{1 + p^{*2}}$ is the Lorentz factor. The dimen-
 311 sionless magnetic matrix \mathbf{B}^* ^[38] is written as

$$312 \quad \hat{\mathbf{B}}^* = \begin{pmatrix} 0 & B_z^* & -B_y^* \\ -B_z^* & 0 & B_x^* \\ B_y^* & -B_x^* & 0 \end{pmatrix}. \quad (17)$$

313 To illustrate the system evolution, the parameters are set as
 314 follows: background magnetic field $B_0 = 0.02$ T, wave an-
 315 gular frequency $\omega_s = 1.5\omega_0$ where $\omega_0 = eB_0/m_0$, wavevec-
 316 tor $\mathbf{k} = 10^5$ m⁻¹, electric field component of the electro-
 317 magnetic wave $E_w = 9$ V/m. The induced wave propagates
 318 along the z axis with linear polarization, and the electrostatic
 319 field is $E_0 = -2.5$ V. The time step is chosen to satisfy
 320 $\Delta t = \min \left(\frac{2\pi}{50(\mathbf{k} \cdot \mathbf{v})}, \frac{2\pi}{50\omega_0}, \frac{2\pi}{50\omega_s} \right)$ to ensure simulation accuracy.

321 The evolution of the electron's motion is shown in Fig. 5.
 322 As the electron accelerates from rest in the electrostatic field
 323 (Fig. 5(b)), the resonant frequencies increase simultaneously
 324 (Fig. 5(a)). The change in parallel velocity caused by the
 325 electromagnetic wave can be quantified as $\Delta v = v_z - v_{zE_0}$
 326 (Fig. 5(c)), where v_z represents the parallel velocity under the
 327 combined fields, while v_{zE_0} denotes the parallel velocity result-
 328 ing solely from the electrostatic field, which can be calculated
 329 as

$$330 \quad v_{zE_0} = \frac{eE_0 t}{m_0 \sqrt{1 + \left(\frac{eE_0 t}{m_0 c} \right)^2}}. \quad (18)$$

331 The cyclotron velocity is shown in Fig. 5(d). The work
 332 done by the electromagnetic wave is shown in Fig. 5(e),
 333 which can be calculated by integrating the power over time
 334 as $E_{||\text{emw}} = \int P_{||\text{emw}} dt$, where $P_{||\text{emw}} = -e(\mathbf{v}_\perp \times \mathbf{B}_{\perp\text{emw}}) \cdot \mathbf{v}_z$.
 335 Since all discrete data points are available from the simulation,
 336 numerical integration is straightforward. Figure 5(f) shows the
 337 gyrokinetic energy evolution over time, where $E_\perp = \frac{1}{2}m_e v_\perp^2$.

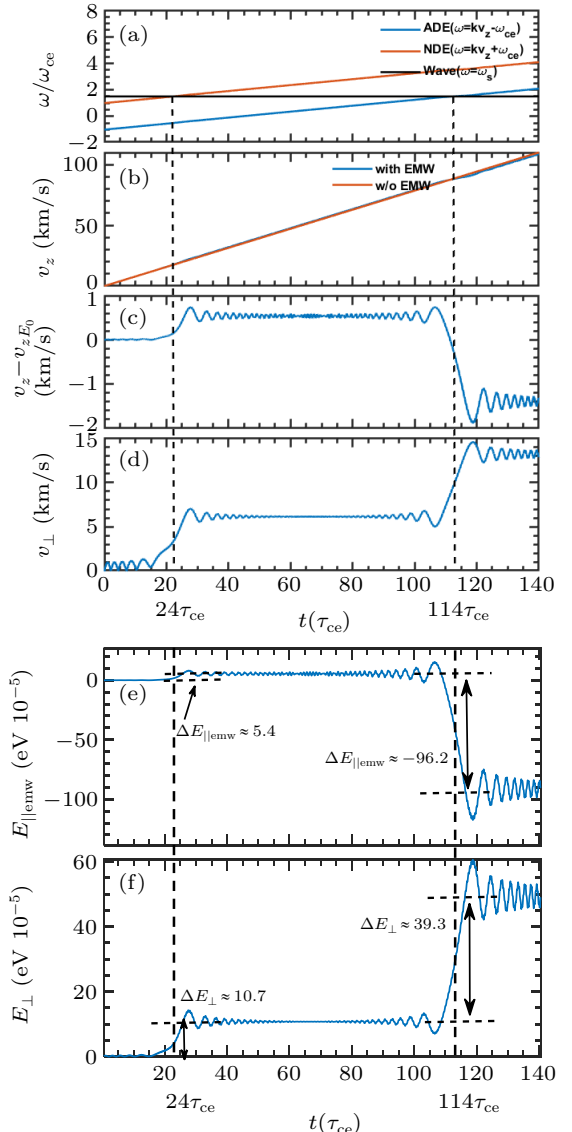


Fig. 5. Kinetic evolution of electrons in a magnetic field under the influence of an electromagnetic wave during acceleration. (a) Frequencies of ADE, NDE, and the source wave. (b) Parallel velocity v_z with and without the electromagnetic wave. (c) Change in parallel velocity induced by the electromagnetic wave. (d) Cyclotron velocity v_\perp . (e) Parallel kinetic energy transferred to the electron by the electromagnetic wave. (f) Evolution of gyro-kinetic (perpendicular) energy.

3.2. Validation of energy transfer ratio

341 As shown in Fig. 5(a), around $23\tau_{ce}$, the normal Doppler
 342 frequency matches that of the induced wave, resulting in a
 343 rapid increase in the cyclotron velocity v_\perp (Fig. 5(b)). Si-
 344 multaneously, the change in parallel velocity induced by the
 345 electromagnetic wave also increases. This behavior can be in-
 346 terpreted as the electron cyclotron system absorbing a photon
 347 during the NDR, leading to an increase in both parallel kinetic
 348 energy and gyro-kinetic energy (internal energy).

349 The change in parallel kinetic energy due to the electro-
 350 magnetic wave is shown in Fig. 5(e), where $\Delta T_{21} = \Delta E_{||\text{emw}} \approx$
 351 5.4×10^{-5} eV. The corresponding increase in gyro-kinetic
 352 energy is $\Delta U_{21} = \Delta E_\perp \approx 10.7 \times 10^{-5}$ eV, also shown in
 353 Fig. 5(e). Consequently, the energy transfer ratio between in-

ternal energy and parallel kinetic energy during resonance is $\frac{\Delta U_{21}}{\Delta T_{21}} \approx 1.98$. According to quantum theory (Eq. 13), for $m = 1$ (NDE) and $k = 10^5 \text{ m}^{-1}$ along the z -axis, the resonant velocity is $v_z \approx 19 \times 10^3 \text{ m/s}$ and $\omega_{ce} \approx 3.51 \times 10^9 \text{ s}^{-1}$. This yields $n_p = 1.85$, in close agreement with the simulation results.

The ADR begins to manifest at $t \approx 113\tau_{ce}$, where $\omega_{ADE} = \omega$ (Fig. 5(a)). At this point, the parallel velocity starts to scatter into the perpendicular direction, as evidenced by the decrease in Δv_z and the corresponding increase in v_\perp (Figs. 5(c) and 5(d)). During the resonant period, the changes in parallel kinetic and gyro-kinetic energies due to the electromagnetic wave are $\Delta T_{21} = \Delta E_{||\text{emw}} \approx -96.2 \times 10^{-5} \text{ eV}$, $\Delta U_{21} = \Delta E_\perp \approx 39.3 \times 10^{-5} \text{ eV}$. The resulting energy transfer ratio is $\frac{\Delta U_{21}}{\Delta T_{21}} \approx -0.408$. According to quantum theory, this ratio is given by $\frac{\Delta U_{21}}{\Delta T_{21}} = -\frac{\hbar\omega_{ce}}{\hbar k \cdot v} \approx -0.3908$, where $\omega_{ce} \approx 3.51 \times 10^9 \text{ s}^{-1}$, $k = 10^5 \text{ m}^{-1}$, and $v_z = 90 \text{ km/s}$. The quantum theory prediction is in good agreement with the numerical results. The derivation of this energy change ratio based on classical theory is provided in the Appendix.

3.3. Validation of the relationship with wave angular momentum

Figures 6(a) and 6(b) show the velocity evolution under linear polarization E_l , right-circular polarization E_R ($m = -1$), and left-circular polarization E_L ($m = 1$). The work done on the electron by the electromagnetic wave, E_{emw} , depicted in Fig. 6(c), comprises the component along the parallel direction, $E_{||\text{emw}}$, as previously described, and the gyro-kinetic energy, $E_{\perp\text{emw}}$. The latter is calculated as $E_{\perp\text{emw}} = \int \mathbf{F}_\perp \cdot \mathbf{v}_\perp dt$, where \mathbf{F}_\perp is determined from the electric and magnetic field forces, and \mathbf{v}_\perp represents the cyclotron velocity. All these quantities can be obtained directly from the numerical results and integrated discretely.

The three polarization types are investigated under the same scenario as before. As a result, the right-hand circularly polarized (RHCP) wave ($m = 1$) induces a velocity change only around $23\tau_{ce}$, whereas the left-hand circularly polarized (LHCP) wave ($m = -1$) induces a velocity change only around $113\tau_{ce}$. This confirms that the RHCP wave corresponds to the NDE, while the LHCP wave corresponds to the ADE, in agreement with the quantum analysis.

For a LHCP electromagnetic wave, the angular momentum selection rule ($m = -1$) restricts resonance to occur only when $\omega = \mathbf{k} \cdot \mathbf{v} - \omega_{ce}$, as confirmed numerically in Fig. 7. This represents a significant departure from previous classical treatments (Eqs. (36) and (37)),^[41] which allowed resonance at arbitrary integer harmonics m , while remaining fully consistent with quantum angular momentum conservation principles.

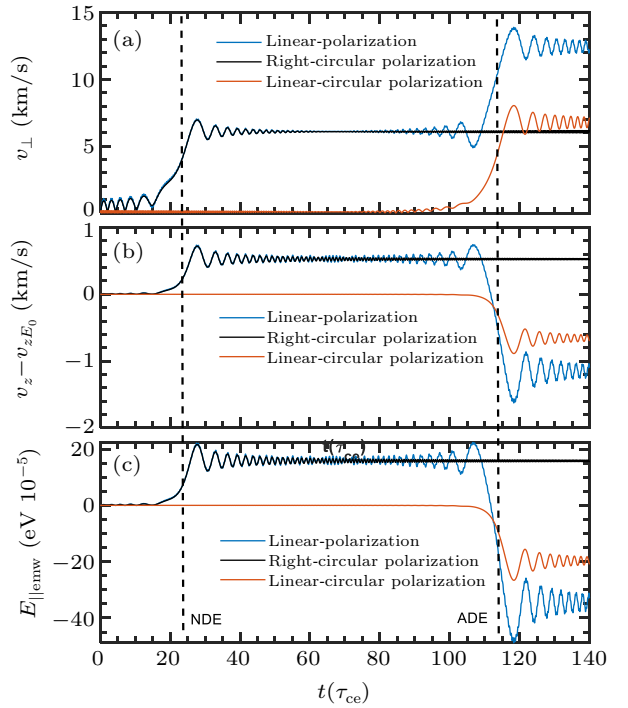


Fig. 6. Velocity evolution induced by waves with linear, right-circular, and left-circular polarization. (a) Cyclotron velocity v_\perp . (b) Change in parallel velocity caused by the electromagnetic wave. (c) Energy $E_{||\text{emw}}$ and $E_{\perp\text{emw}}$.

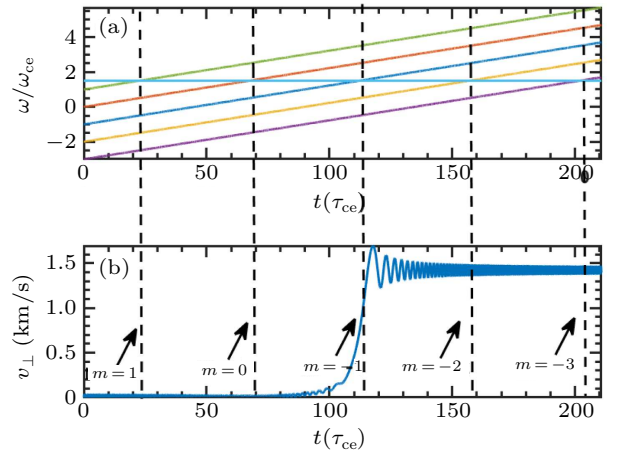


Fig. 7. (a) Frequency $\omega = \mathbf{k} \cdot \mathbf{v} + m\omega_{ce}$ for different m values and induced wave frequencies. (b) Evolution of perpendicular velocity under a left-circularly polarized wave ($m = -1$).

4. Discussion

Based on momentum and angular momentum conservation, let us consider the case where \mathbf{k} is oriented opposite to \mathbf{v}_\parallel (or \mathbf{B}_0). In this scenario, if a cyclotron electron emits a photon with left-hand circular polarization and momentum $-\hbar\mathbf{k}$, carrying angular momentum \hbar , then after emission the change in internal energy is $\Delta U = -\hbar\omega_{ce} < 0$, while the change in translational kinetic energy is $\Delta T = \hbar k v_\parallel > 0$. In contrast, if the emitted photon has right-hand circular polarization with momentum $-\hbar\mathbf{k}$, the change in internal energy becomes $\Delta U = \hbar\omega_{ce} > 0$, while the translational kinetic energy remains $\Delta T = \hbar k v_\parallel > 0$. This scenario would violate energy

conservation, since an electron cannot emit a photon while simultaneously increasing its total energy. Consequently, for a plane electromagnetic wave, only the left-circularly polarized component can resonate with an electron moving opposite to v_{\parallel} (or B_0).

The resonant condition can also be interpreted classically. In the case of ADR, where $\mathbf{k} \parallel \mathbf{v}$ and $v_z > c' \equiv \omega/|\mathbf{k}|$, the LHCP wave appears as a right-hand polarized wave in the cyclotron electron's rest frame, allowing resonance. In contrast, for Normal Doppler Resonance, where $v_z < c'$, the RHCP wave maintains its polarization in the electron's rest frame. However, when \mathbf{k} is anti-parallel to \mathbf{v} ($\mathbf{k} \cdot \mathbf{v} < 0$), only the LHCP wave preserves the same rotational direction as the electron's cyclotron motion, independent of the parallel velocity. Therefore, in this configuration, only left-hand polarized waves can resonate with the electron.

This study also provides a perspective on electron heating and current drive by EM waves. During the NDR process, the fraction of the electron's internal energy gain from the EM wave relative to the total absorbed wave energy can be expressed as $\eta_H = \frac{m\omega_{ce}}{\omega}$, while the fraction contributing to parallel kinetic energy is $\eta_T = \frac{\mathbf{k} \cdot \mathbf{v}}{\omega}$. These relations can help optimize plasma heating and current drive efficiency. In the case of ADR, the electron's parallel kinetic energy can be converted into internal (gyro) energy, a mechanism that may contribute to suppressing runaway electron energies. This phenomenon has been studied previously^[11,22], but further investigation is warranted in future fusion tokamak plasmas.

5. Conclusion

This paper presents a simple yet effective approach for analyzing resonant processes associated with the NDE and ADE. By combining quantum theory with angular momentum conservation analysis, it is demonstrated that the parameter m in the resonance condition $\omega = \mathbf{k} \cdot \mathbf{v} + m\omega_{ce}$ directly corresponds to the angular momentum of the resonant wave. Numerical simulations based on the Volume-Preserving Algorithm (VPA) further support the quantum results, confirming both the angular momentum interpretation of m and the energy transfer characteristics. Future work will investigate the interaction between electron energy transformation and helicon waves in a plasma environment, aiming to provide deeper insights into applications such as plasma heating^[40] and suppression of runaway electrons.

Appendix A: Classical analysis of anomalous Doppler resonance

Neglecting the static electric field and relativistic effects, we provide a brief derivation of the energy transformation pro-

cess based on classical dynamical equations

$$m_e \frac{d\mathbf{v}_{\parallel}}{dt} = -e(\mathbf{v}_{\perp} \times \mathbf{B}_{\perp}), \quad (\text{A1})$$

$$m_e \frac{d\mathbf{v}_{\perp}}{dt} = -e(\mathbf{v}_{\perp} \times \mathbf{B}_0 + \mathbf{v}_{\parallel} \times \mathbf{B}_{\perp} + \mathbf{v}_{\perp} \times \mathbf{B}_0). \quad (\text{A2})$$

Consider $\mathbf{B}_{\perp} = \frac{e_k \times \mathbf{E}_{\perp}}{v_p}$, where e_k is the unit vector along the wave vector of the electromagnetic wave, which is along the z -axis. Taking the dot product of \mathbf{v}_{\parallel} and \mathbf{v}_{\perp} with Eqs. (A1) and (A2), and substituting \mathbf{B}_{\perp} , we obtain

$$m_e \mathbf{v}_{\parallel} \cdot \frac{d\mathbf{v}_{\parallel}}{dt} = -e(\mathbf{v}_{\perp} \cdot \mathbf{E}_{\perp}) \frac{v_{\parallel}}{v_p}, \quad (\text{A3})$$

$$m_e \mathbf{v}_{\perp} \cdot \frac{d\mathbf{v}_{\perp}}{dt} = e(\mathbf{v}_{\perp} \cdot \mathbf{E}_{\perp}) \frac{v_{\parallel}}{v_p} - e(\mathbf{v}_{\perp} \cdot \mathbf{E}_{\perp}). \quad (\text{A4})$$

Here, $v_p = \omega/k$ is the phase velocity of the wave. Adding Eqs. (A3) and (A4) gives the total energy change of the electron

$$\frac{d}{dt} \left(\frac{1}{2} m_e v_{\parallel}^2 + \frac{1}{2} m_e v_{\perp}^2 \right) = -e(\mathbf{v}_{\perp} \cdot \mathbf{E}_{\perp}). \quad (\text{A5})$$

The sign of $-e(\mathbf{v}_{\perp} \cdot \mathbf{E}_{\perp})$ determines whether the electromagnetic (E.M.) wave undergoes "emission" ($-e(\mathbf{v}_{\perp} \cdot \mathbf{E}_{\perp}) < 0$) or "absorption" ($-e(\mathbf{v}_{\perp} \cdot \mathbf{E}_{\perp}) > 0$), depending on the phase difference between v_{\perp} and E_{\perp} .

From Eq. (A4) we have

$$e(\mathbf{v}_{\perp} \cdot \mathbf{E}_{\perp}) = \frac{m_e \mathbf{v}_{\perp} \cdot \frac{d\mathbf{v}_{\perp}}{dt}}{\frac{v_{\parallel}}{v_p} - 1}. \quad (\text{A6})$$

Substituting Eq. (A6) into Eq. (A3), we obtain

$$m_e \mathbf{v}_{\parallel} \cdot \frac{d\mathbf{v}_{\parallel}}{dt} = -\frac{m_e \mathbf{v}_{\perp} \cdot \frac{d\mathbf{v}_{\perp}}{dt}}{\frac{v_{\parallel}}{v_p} - 1} \frac{v_{\parallel}}{v_p}. \quad (\text{A7})$$

Integrating Eq. (A7), we obtain the classical invariant of motion for the electron under ADR

$$\frac{1}{2} m_e \left(v_{\parallel} - \frac{\omega}{k} \right)^2 + \frac{1}{2} m_e v_{\perp}^2 = C_0, \quad (\text{A8})$$

where C_0 is a constant determined by the initial conditions.

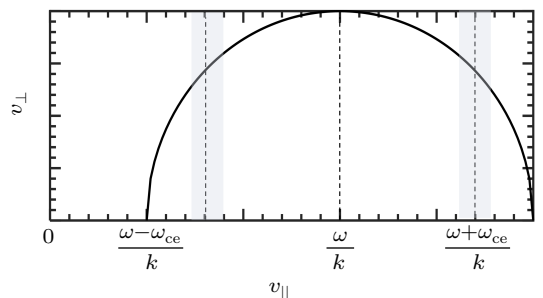


Fig. A1. Trajectory in the $(v_{\parallel}, v_{\perp})$ plane.

Here, C_0 refers to the initial value. The change in velocity is constrained to a circular trajectory, as illustrated in Fig. A1.

At the NDR, where

$$v_{\parallel} = \frac{\omega - \omega_{ce}}{k},$$

495 an increase in v_{\parallel} corresponds to an increase in v_{\perp} . In contrast,
 496 at the ADR, where

$$497 \quad v_{\parallel} = \frac{\omega + \omega_{ce}}{k},$$

498 an increase in v_{\parallel} corresponds to a decrease in v_{\perp} .

499 The change of energy in translational energy and gyro-
 500 kinetic energy can be written as:

$$501 \quad \frac{\Delta U}{\Delta T} = \frac{v_{\perp} dv_{\perp}}{v_{\parallel} dv_{\parallel}}. \quad (A9)$$

502 From Eq. (A8), we have

$$503 \quad \frac{dv_{\perp}}{dv_{\parallel}} = -\frac{v_{\parallel} - \frac{\omega}{k}}{v_{\perp}}. \quad (A10)$$

504 Combining Eqs. (A9) and (A10), we obtain

$$505 \quad \frac{\Delta U}{\Delta T} = -\frac{v_{\parallel} - \frac{\omega}{k}}{v_{\parallel}}. \quad (A11)$$

506 According to the resonant condition

$$507 \quad \omega = k v_{\parallel} + m \omega_{ce},$$

508 substituting v_{\parallel} into Eq. (A11) yields:

$$509 \quad \frac{\Delta U}{\Delta T} = \frac{m \omega_{ce}}{kv_{\parallel}}, \quad (A12)$$

510 which agrees with the quantum result in Eq. (12).

511 Acknowledgment

512 This project is supported by the National Magnetic
 513 Confinement Fusion Energy Program of China (Grant
 514 No. 2019YFE03020001).

515 References

- 516 [1] Tamm I E 1959 *Nobel Lectures* **18** 122
- 517 [2] Frank I M 1960 *Science* **131** 702
- 518 [3] Kiang D and Young K 2008 *Am. J. Phys.* **76** 1012
- 519 [4] Ginzburg V L 1960 *Sov. Phys. Usp.* **2** 874
- [5] Shustin E G, Popovich P and Kharchenko I F 1971 *Sov. Phys. JETP* **59** 657
- [6] Nezlin M V 1976 *Sov. Phys. Usp.* **19** 946
- [7] Santini F, Barbato E and De Marco F 1984 *Phys. Rev. Lett.* **52** 1300
- [8] Kho T H and Lin A T 1988 *Phys. Rev. A* **38** 2883
- [9] Liu J, Wang Y and Qin H 2016 *Nucl. Fusion* **56** 064002
- [10] Wang Y, Qin H and Liu J 2016 *Phys. Plasmas* **23** 062505
- [11] Guo Z, McDevitt C J and Tang X Z 2018 *Phys. Plasmas* **25** 032504
- [12] Liu C, Hirvijoki E and Fu G Y 2018 *Phys. Rev. Lett.* **120** 265001
- [13] Shi X, Lin X and Kaminer I 2018 *Nat. Phys.* **14** 1001
- [14] Filatov L V and Melnikov V F 2021 *Geomagn. Aeron.* **61** 1183
- [15] Artsimovich L A, Bobrovskii G A and Mirnov S V 1967 *Sov. At. Energ.* **22** 325
- [16] Kadomtsev B B and Pogutse O P 1968 *Sov. Phys. JETP* **26** 1146
- [17] Spong D A, Heidbrink W W and Paz-Soldan C 2018 *Phys. Rev. Lett.* **120** 155002
- [18] Liu Y, Zhou T and Hu Y 2019 *Nucl. Fusion* **59** 106024
- [19] Gorozhanin D V, Ivanov B I and Khoruzhii V M 1997 *Waves excitation at anomalous Doppler effect for various electron beam energies*, Dec 31, 1997, Japan, pp. 402
- [20] Sajjad S 2007 *Chin. Phys. Lett.* **24** 3195
- [21] Castejon F and Eguilior S 2003 *Particle Dynamics under Quasi-linear Interaction with Electromagnetic Waves* (Madrid: Centro de Investigaciones Energeticas) p. 4
- [22] Zhang Q, Zhang Y, Tang Q and Tang X Z 2024 arXiv:2409.15830 [physics.plasm-ph]
- [23] Ginzburg N S 1979 *Radiophys. Quantum Electron.* **22** 323
- [24] Ginzburg V L 1996 *Phys. Usp.* **39** 973
- [25] Ginzburg V L 2005 *Acoust. Phys.* **51** 11
- [26] Coppi B, Pegoraro F, Pozzoli R and Rewoldt G 1976 *Nucl. Fusion* **16** 309
- [27] Frolov V P and Ginzburg V L 1986 *Phys. Lett. A* **116** 423
- [28] Arnaut H H and Barbosa G A 2000 *Phys. Rev. Lett.* **85** 286
- [29] Liu H, He X T, Chen S G and Zhang W Y 2004 arXiv:physics/0411183 [physics.plasm-ph]
- [30] Qian B L 1999 *IEEE Trans. Plasma Sci.* **27** 1578
- [31] Weyssow B 1990 *J. Plasma Phys.* **43** 119
- [32] Gogoberidze G and Machabeli G Z 2005 *Mon. Not. R. Astron. Soc.* **364** 1363
- [33] Roberts C S and Buchsbaum S J 1964 *Phys. Rev.* **135** A381
- [34] Bourdier A and Gond S 2000 *Phys. Rev. E* **62** 4189
- [35] Nusinovich G S, Korol M and Jerby E 1999 *Phys. Rev. E* **59** 2311
- [36] Nusinovich G S, Latham P E and Dumbrabs O 1995 *Phys. Rev. E* **52** 998
- [37] Qian B L 2000 *Phys. Plasmas* **7** 537
- [38] Zhang R, Liu J, Qin H, Wang Y, He Y and Sun Y 2015 *Phys. Plasmas* **22** 044501
- [39] Sha W E I, Lan Z, Chen M L N, Chen Y P and Sun S 2024 *IEEE J. Multiscale Multiphys. Comput. Tech.* **9** 113
- [40] Zhao Y, Bai J, Cao Y, Wu S, Ahedo E, Merino M and Tian B 2022 *Chin. Phys. B* **31** 075203
- [41] Dendy R O 1987 *Phys. Fluids* **30** 2438